The DOI for this manuscript is doi: .

Please use the following full citation:

Yu, L., Tang, L., Yang, T.: Experimental investigation of a passive self-tuning resonator based on a beam-slider structure. Acta Mechanica Sinica., doi: , in press.

Experimental investigation of a passive self-tuning resonator based on a beam-slider structure

Liuding Yu[1, 2], Lihua Tang[2,*], Tiejun Yang[1]

1. *Power and energy engineering college, Harbin Engineering University, Harbin 150001, China*
2. *Department of mechanical engineering, University of Auckland, Auckland 1010, New Zealand*

Abstract

This work investigates a self-tuning resonator composed of a slender clamped-clamped steel beam and a freely movable slider. The clamped-clamped beam exhibits hardening nonlinearity when it vibrates in large amplitude, providing a broad bandwidth of dynamic response. The moving slider changes the mass distribution of the whole structure and provides a passive self-tuning approach for capturing the high energy orbit of the structure. In the case without inclination, adequate inertial force that mainly depends on the vibration amplitude of beam and the position of the slider can drive the slider to move from the side toward the centre of the beam. This movement amplifies the beam response when the excitation frequency is below 37 Hz in our prototyped device. In the multi-orbit frequency range (28 Hz-37 Hz), the self-tuning and magnification of beam response can be achieved when the slider is initially placed in an appropriate position on the beam. Once the beam is disturbed, however, the desired response in the high energy orbit can be lost easily and cannot be reacquired without external assistance. In an improved design with a small inclination, the introduced small gravitational component enables the slider to move from higher side toward the lower side when the beam amplitude is small. This property sacrifices the less efficient self-tuning region below 25 Hz but can enable the beam to acquire and maintain the high energy orbit response in the multi-orbit frequency range (28 Hz-39 Hz), which is resistant to disturbance. The proposed resonator in this paper not only broadens the frequency bandwidth of dynamic response but also enable to capture and maintain high energy orbit in a completely passive way. Such a passive self-tuning structure has the advantage in the design of broadband vibration energy harvesting systems.

Keywords Passive self-tuning, Vibration energy harvester, Nonlinearity, Beam-slider structure

* Corresponding author. Email , l.tang@auckland.ac.nz

1. Introduction

Harvesting vibrational energy from environments has received wide research attention in recent years. Vibration sources may change frequency over time. A linear harvester with a narrow operation frequency bandwidth around resonance has deteriorated performance once the excitation frequency is detuned from the resonance[1].

Nonlinear vibration structures have the advantage for broadening the dynamic response of harvesters [2]. However, the broadband performance is achieved only when the oscillators could capture the high energy orbit, which strongly depends on the excitation level and initial conditions [3-6]. Researchers proposed various methods to trigger nonlinear systems to capture and maintain the high energy orbit and thus vibrate in a large amplitude to enable efficient energy conversion. Zhou et al. [7] introduced a mechanical impact as additional kinetic energy to obtain the high energy orbit. The effective bandwidth of bistable and tristable energy harvesters increased from 3 Hz and 5 Hz to 15 Hz and 12 Hz when excitation level was 0.27 g, respectively. Wang et al. [8] added an elastic magnifier between the bistable piezoelectric harvester and excitation base to broaden the frequency band and enhance the maximum output performance. Large mass and stiffness ratios are demanded to trigger high energy orbit, which however might not be feasible in practice due to the weight and space constraints of the bistable harvesters. Considering that the electromagnetic and piezoelectric elements in energy harvesters can also be used as actuators, the load circuits can be switched to be excitation circuits to assist the oscillators to catch the high energy orbits. Mallick et al. [9] proposed an electric magnet to couple with the hardening Duffing mechanical system to surf high energy output branch. However, the possibility of successful switching to the high energy orbit depended on the supplied sinusoidal voltage parameters in terms of amplitude, frequency and phase. The mapping for successful and unsuccessful switching was interlaced intricately. Masuda et al. [10] proposed a method to switch the load circuit from the conventional mode to the excitation mode when the Duffing-type electromagnetic harvester amplitude decreases. The theoretical and numerical analysis was carried out and confirmed that the circuit induced self-excitation could destabilized the low energy orbit. For piezoelectric energy harvesters, Sebald et al. [11, 12] presented that both the output energy and frequency bandwidth of the Duffing type energy harvesters could be improved. By applying a fast burst perturbation on the piezoelectric element, the oscillator was able to catch the high energy orbit with a very small energy cost. Lan et al. [5] developed a negative resistance circuit to generate a voltage impulse perturbation, which could trigger and maintain high energy orbit for both monostable and bistable nonlinear piezoelectric energy harvesters.

On the other hand, concepts of resonance tuning have been exploited in the literature for efficiency improvement. The energy consumption in the tuning system should be minimized or completely passive. Otherwise, the gain of energy harvesting performance might be sacrificed. Gu et al. [13] proposed a passive self-tuning piezoelectric cantilever beam installed in the radial orientation on the rotary machine. The centrifugal force that changes the resonance frequency of the harvester varies with the rotational speed, providing the frequency self-tracking and self-tuning capability in a wide speed range. Jo et al. [14] proposed a flexible PVDF seesaw structure for transverse vibration energy harvesting. The resonance frequency could be automatically switched and maintained by changing the length of each arm of the seesaw structure passively. Experimental results demonstrated its capacity of switching resonance frequency from 10 Hz to 40 Hz in real time without external energy consumption. A beam-slider structure was experimentally proved to be passively self-tuning by Millar [15]. The theoretical model was established by Hamilton's Principle to illustrate the dynamics of the beam and the slider. Experiment and simulation results showed its capability in passive self-tuning in a wide frequency range. Further experimental investigation of such a beam-slider structure was conducted in Ref. [16]. 60 mm long steel and Beryllium copper beam were used to contrast with 300 mm aluminum beam. The results proved that the beam-slider structure could achieve self-tuning and maintain its tuned state as frequency swept up and down even though the device was scaled down. Pillatstch et al. experimentally investigated the self-tuning behavior of two types (steel and Beryllium copper) of clamped-clamped beam with the sliding proof mass. The nonlinearities of the clamped-clamped beams without the slider have been studied by downward and forward sweep frequency excitation. But the effect of large proof mass outweighs the effect of the nonlinearity for broadening the bandwidth [17]. Discrepancy in beam displacement and output voltage were observed when piezoelectric patches were bonded to the clamped-clamped beam in Ref. [18]. The characteristics of beam-slider structure were proved to be sensitive to parameters such as mass, gap size, etc., giving five distinct cases of behavior. Staaf et al. [19, 20] coupled two piezoelectric cantilevers by using a connecting beam which carrying a free-sliding mass to make up a 4-DOF self-tuning energy harvester. The experimental results showed that the harvester was imparted with the capacity of passive self-tuning. The further eigen-frequency analysis suggested that the asymmetric system caused by two different length of piezoelectric cantilever beam could achieve broader bandwidth. Krack et al. [21] established the mathematical model by simplifying the contact condition between the slider and beam as four-point contact and investigated the self-adaptive dynamics. Simulation results qualitatively illustrated the improved performance of the

adaptive system, tuning frequency dependence on the slider location and the limitation of the operating regime. Krack et al. [21] mainly focused on the properties of self-tuning and the dynamics of the sliding mass. Their mathematical model neglected the beam nonlinearity and did not reveal the essence of the self-tuning principle.

In this work, we investigate the passive self-tuning process of the clamped-clamped beam-slider structure with nonlinearity. This work aims to reveal the role of the slider in self-tuning process and understand the interaction between the motion of the slider and the response of the beam. The operation range for self-tuning of the beam-slider structure is investigated experimentally. It is found that the role of the slider is mainly on helping capture the large amplitude orbit which inherently exists in the clamped-clamped beam with nonlinearity. Two cases without and with inclination have been considered and compared. The later improves the self-tuning region by introducing a small gravitational component. The rest of the paper is organized as follows: Section 2 briefs the working principle of the nonlinear clamped-clamped beam-slider structure. Section 3 presents the experimental setup and methodology. Section 4 presents the sweep frequency responses of the beam with mass fixed. Section 5 presents the behavior of the nonlinear beam and the slider when the structure installed without inclination. Section 6 discusses the improved self-tuning capability of the beam-slider structure when it is installed with a small inclination. The comparison between the two cases is given at the end of this section. Section 7 concludes the main findings of this work.

2. Working Principle

The beam-slider structure is composed of a clamped-clamped beam and a free movable slider, as shown in Fig. 1(a). Because the beam used in this study is a slender beam, the geometric hardening nonlinearity caused by stretching strain cannot be neglected [22]. This nonlinear beam contributes the wide frequency bandwidth for the system. When the structure is driven by the base excitation, on one hand, the transverse vibration of the beam carries the slider to vibrate in *w* direction; on the other hand, the slider may move along the beam.

To explain the motion of the slider along the beam in the view of non-inertial reference frame (the beam), the inertial force must be introduced. As shown in Figs. 1(b) and (c), the inertial force applied on the slider is $F_i = -Ma_b$, where M is the mass of the slider and a_b is the acceleration of the beam at the position of the slider. The inertial force F_i is always normal to the equilibrium position of the beam, which is not purely vertical if a small inclination is

introduced to the base excitation. Apart from F_i, there are another two forces applied on the slider, that is, the normal force F_n and gravity G. Obviously, the total force F_T of F_n, F_i and G is along the beam and it is actually contributed by the components of F_i and G along the beam, which determine the direction of movement of the slider.

For the case without inclination ($\theta = 0°$), when the beam is below the equilibrium position, the components of G and F_i along the beam are aligned. Thus the total force F_T always points to the centre of the beam (Fig. 1(b)). However, when the beam is above the equilibrium position, it is not obvious to determine the direction of F_T. It points to the centre of the beam if $F_i > G$ or to the fixed end of the beam if $F_i < G$. Even though the direction of F_T is uncertain when the beam is above the equilibrium, it is definite that the value of F_T below the equilibrium will be larger than that at the same position above the equilibrium. Therefore, in each vibration period, overall behavior of the slider is that it moves toward the centre of the beam.

For the case with small inclination introduced ($\theta \neq 0°$), the base excitation is still normal to the beam. When the slider is located on the higher half side of the beam, it will benefit from the inclination θ and move toward the beam centre. However, when the slider is located on the lower half side of the beam, even when the beam is below the equilibrium, the direction of F_T does not always point to the centre. This is because the components of the G and F_i along the beam are not necessarily aligned. When the vibration amplitude is small, F_T could point toward the end of the beam (Fig. 1(c)). This is different from the case without inclination. As a result, the duration for F_T pointing toward the centre in one vibration period deceases. In addition, the value of F_T below the beam equilibrium position is smaller than that in the case without inclination given the same beam displacement. As a result, the slider on the lower half side of the beam needs larger F_i to move toward the centre. If the vibration amplitude is not large enough and thus F_i is insufficient, the slider will move back to the lower end of the beam. It is actually intuitive that the slider in the lower side of the beam is more difficult to move toward the centre upward.

What is more, because of the existence of friction in reality, the total force F_T also needs to be large enough to overcome the maximum static friction force for driving the slider to move. Otherwise, the slider will keep still at the initial position.

In summary, the inclination and the beam vibration amplitude at the position of the slider determine the total force F_T and thereby determine the movement of the slider. The movement of the slider changes the mass distribution of the system and thus shift the natural frequency of the beam and its dynamic response. Conversely, the shift of the response of the beam in

turn affects the motion of the slider. This interaction of the beam and the slider is the key of the passive tuning process of the system. The detailed explanation on this interaction and the consequent behaviors of the beam and slider will be given in the discussion of the experimental results in Sections 5 and 6.

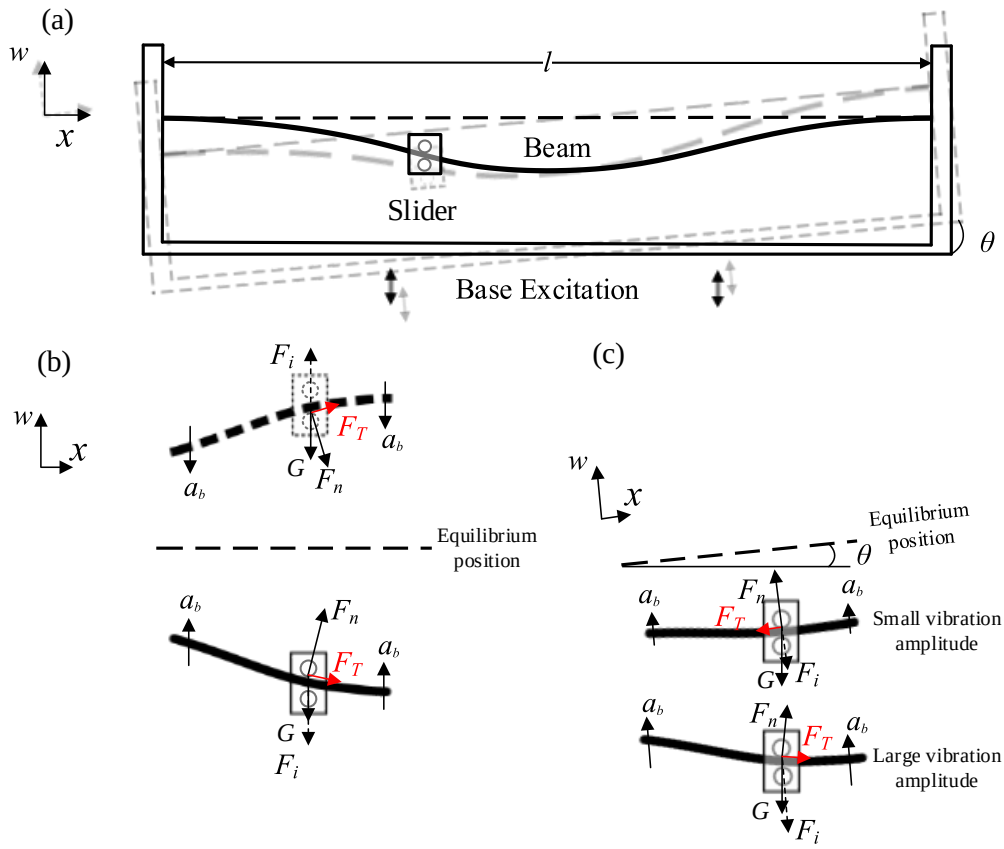

Fig.1 (a) Beam-slider structure diagram; (b) free body diagram of slider in vibration without inclination and (c) free body diagram of slider in vibration with inclination

3. Experimental Setup and Methodology

The experimental setup and beam-slider structure prototype are shown in Figs. 2(a) and (b), respectively. To ensure that the slider could move smoothly along the beam, a mass assembled with small bearings was used as the slider. The total weight of the slider was 18.42 g. A stainless steel beam of 270 mm × 20 mm × 0.5 mm was used in the experiment. The beam-slider structure was tested on an electrodynamic shaker (DP V100 Air Cooled Shaker, Data Physics Corporation). The shaker was controlled by a controller (SignalStar Scalar, Data Physics Corporation) with a single axis accelerometer (352A56, PCB PIZOTRONICS) to provide feedback. The shaker could be adjusted to have an inclination and excite in a non-vertical direction. One laser displacement sensor (CP08MHT80, Wenglor Sensoric

GmbH) was used to measure the beam displacement (w_c) at the point that is 10 mm away from the centre of the beam to avoid the blockage of laser measurement when the slider reaches the centre. The data acquisition module (NI9215, National Instrument) was used to acquire and process the displacement signal. The time history of the slider trajectory during self-tuning process was recorded by a high speed video camera fastened above the beam-slider structure.

The experiment was conducted for two cases: the case without the inclination ($\theta = 0°$) and the case with inclination ($\theta = 3°$). The first case was mainly designed to investigate the mechanism of the tuning process. The second case was an improved system in which some drawbacks of the first case can be overcome and achieve robust self-tuning. In each case, two types of experiment were conducted. For the first type of experiment, the slider was fixed on the beam in different positions. Frequency response functions (FRFs) which can exhibit the beam nonlinear properties were acquired by forward and backward sine sweep excitation. For the second type of experiment, the slider was free to move along the beam and the system was excited at a single frequency. The trajectories of the slider and the responses of the beam were recorded by video camera and laser displacement sensor, respectively. In both experiments, the base excitation level was kept at 10 m s^{-2}. The frequency sweeping rate is 0.2 Hz s^{-1}. The second type experiment obtained the behavior of the beam and the slider, which could be explained by the steady state response of the first type experiment with fixed mass. They supplied not only the details about how the self-tuning process was achieved but also the interaction between the beam and slider.

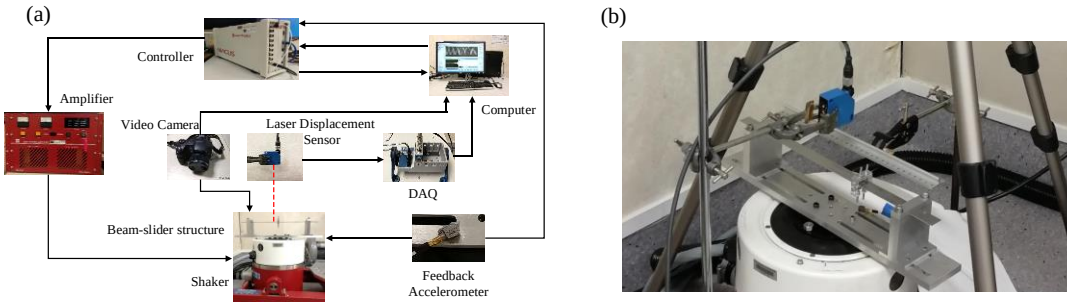

Fig.2 (a) Experimental setup and (b) Beam-slider structure prototype

4. Sweep Frequency Response Function with Fixed Mass

When the slider stops at the certain position in the final stable state, i.e. the velocity and acceleration of the slider are zero, it suggests that the beam-slider structure can be regarded as a nonlinear beam carrying a fixed lumped mass. The FRF of the beam varies when the slider stops in different positions of the beam, which is closely related to the self-tuning mechanism.

Hence, the sweep FRFs are first determined by fixing the slider at different positions on the beam, as shown in Fig. 3(a). The position of the slider fixed on the beam to the clamp is denoted by a normalized parameter $\lambda=s/l$. Here, since the slider is fixed during the sweep frequency response analysis, the slider is called “fixed mass”. Since the horizontal beam was symmetric, the position of the slider is only varied along left half of the beam (λ=0.019-0.5).

The clamped-clamped beam possesses the hardening nonlinearity. As a result, as shown in Fig. 3(a), forward sweep and backward sweep responses do not coincide and they jump at different frequencies. The forward sweep jumps down from the high energy orbit at a higher frequency (f_f) and the backward sweep jumps up at a lower frequency (f_b). Between f_b and f_f, the low energy orbit (dashed line) and high energy orbit (solid line) coexist. The orbit that the system could capture depends on the initial conditions. There are various methods on perturbing the system from the low energy orbit to high energy orbit in the literature [5, 7, 9, 10]. Out of this range, the forward and backward sweep frequency responses coincide and only one orbit exists.

When the position of the fixed mass is varied from the clamping end (λ=0.019) to the centre of the beam (λ=0.5), both f_b and f_f decrease, as shown in Fig. 3(a). When the fixed mass is located at the centre, the system has the lowest jump up and jump down frequencies, i.e., f_b =28 Hz and f_f =43 Hz. On the contrary, the highest jump up and jump down frequencies, i.e., f_b=45 Hz and f_f=58 Hz, are obtained when the fixed mass is located at the clamping end of the beam (λ=0.019).

For each position that the mass is fixed, the sweep FRFs will experience unique orbit, multi-orbits and unique orbit in succession as excitation frequency increases. However, from another perspective, when the excitation is at a fixed frequency but with varying mass positions, the stable response appears to be more complicated. In order to illustrate the relation between the beam response and the fixed mass position, the whole frequency band in Fig. 3(a) is classified to five ranges according to the number of energy orbits changes. In Frequency Range A (<28 Hz), the unique orbit exists wherever the mass is fixed. In Frequency Range B (28 Hz~43 Hz), as the fixed mass position varies from the clamping end (λ=0.019) to the centre (λ=0.5), the unique orbit bifurcates and generates two energy orbits at a certain position. In Frequency Range C (43 Hz~45 Hz), the initial unique orbit is bifurcated to two energy orbits and then merge to a unique energy orbit again when fixed mass is close to the centre. In Frequency Range D (45 Hz~58 Hz), two energy orbits coexist when the mass is at the clamping end of the beam (λ=0.019), and the two orbits will merge to one orbit beyond a certain point. In Frequency Range E (>58 Hz), similar to Frequency Range A, only

one orbit exists.

Five frequencies are chosen to represent the beam response transformation when the orbits change in the five frequency ranges, as shown in Fig. 3(b). The black solid-dotted line (24 Hz) represents Frequency Range A. The reason why beam response in unique orbit increases is that the natural frequency of beam-slider structure get closer to the excitation frequency (24 Hz) when the fixed mass located closer to the centre and thus the response increases. The red solid-dotted and dash-dotted line (38 Hz), representing Frequency Range B, shows that the bifurcation occurs when the fixed mass is located around λ=0.2. After that, the unique orbit bifurcates to a high energy orbit and a low energy orbit. The amplitude of the high energy orbit will keep growing until the mass is fixed at the centre. Beam response amplitude magnification in this frequency range is more significant. The maximum amplitude at 38 Hz is nearly three times that at 24 Hz. On the contrary, the response in the lower energy orbit will keep decreasing. The pink solid-dotted and dash-dotted line (44 Hz) represents Frequency Range C. As seen in Fig. 3(b), the response bifurcates around λ=0.1 and then the high energy orbit jumps down to the low energy orbit around λ=0.35 rather than keeping growing. Furthermore, because the excitation frequency, 44 Hz, is far away from the natural frequency when the mass is located at the centre, the response is almost unnoticeable. The blue solid-dotted and dash-dotted line (49 Hz), representing Frequency Range D, shows that two energy orbits have already existed when the mass is located at the clamping end of the beam. The two orbits converge around λ=0.15 when the high energy orbit jumps down. The green solid-dotted line (59 Hz) in Fig. 3(b) represents Frequency Range E. The response of the unique orbit is quite small and it decreases when the mass position shifts to the centre. This is because the change in mass position make the natural frequency of beam-slider structure even further away from the excitation frequency (59 Hz).

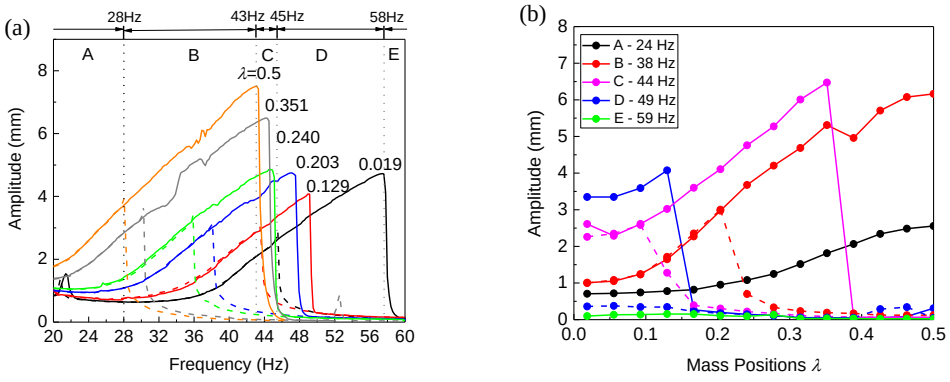

Fig.3 (a) Forward (solid line) and backward (dashed line) sweep frequency responses of w_c when the mass is fixed at λ=0.019 (5 mm from the clamp), 0.129, 0.203, 0.240, 0.351 and 0.5 (the centre of the beam). (b) Vibration

amplitude varies with fixed mass position under single frequency excitation. Solid-dotted and dash-dotted lines are high energy orbits and low energy orbits, respectively.

5. Self-Tuning without Inclination

5.1 Critical initial positions for mass sliding on the beam

To test the self-tuning capability, in this section, the mass is allowed to slide along the beam. Thus, the mass is called “slider”. For each excitation frequency, the slider is placed at different initial positions to observe its trajectory if it can slide and the corresponding beam response (w_c). Fig. 4 shows the various tuning regions in terms of excitation frequency (f_e) and the initial position (λ_0) of the slider. The blue and red dotted lines are the critical initial positions that determine whether the slider can move along the beam toward the centre. The black and orange dashed lines depict the jump up frequency f_b and jump down frequency f_f when the fixed mass is at the corresponding positions from previous sweep frequency experiment in Section 4.1. Interestingly, the critical initial positions (red dotted line) coincide with the boundary of f_b (black dashed line).

Four regions of interest are formed by these lines. Below blue dotted line is Region 1. If the slider is initially placed at a position in this region (near the clamping end of the beam), it cannot move along the beam due to small beam vibration amplitude and less inertia force and thus insufficient F_T along the axial direction to overcome the static friction. In between the blue and red dotted lines is Region 2. If the slider is initially located in this region, it can start sliding toward the centre. Beyond the red dotted line on the right up side (Regions 3 and 4), the slider cannot move. When the slider is initially placed in Region 2, only one energy orbit exists but the vibration amplitude is large enough to provide the slider sufficient inertial force to move. When the slider moves toward the centre passing Region 3, though there are two energy orbits, the relative large amplitude vibration gained from Region 2 will help the beam-slider structure capture the high energy orbit and keep the momentum of the slider to move and eventually reach the centre of the beam. It is thus not difficult to understand why the critical positions (red dotted line) coincide with the boundary of f_b (black dashed line). However, if the slider is initially placed in Region 3, the beam-slider structure will start vibrating from the low energy orbit with low amplitude. Thus, because of the insufficient inertial force and F_T to overcome the friction, the slider will stay still on the beam. In Region 4, since the excitation frequency is far beyond the resonance with small vibration amplitude, the slider cannot move either. In summary, if the beam-slider structure is excited from the

static state, the slider can move toward the centre only when its initial position is in Region 2. Though two energy orbits coexist, the slider cannot move if it is initially placed in Region 3.

These four regions can be further divided into a number of sub-regions by the Frequency Ranges A-E mentioned in Section 4.1. Note, Frequency Ranges A, C, D and E are exactly the same as those in Fig. 3(a). Frequency Range B is further subdivided into two ranges B^{α} and B^{β} at 37 Hz because of the different beam responses though the slider can move toward the centre in both cases. In each sub-region, the different behaviors of beam-slider structure in terms of the beam response and slider trajectory in the time history will be further discussed in the following section.

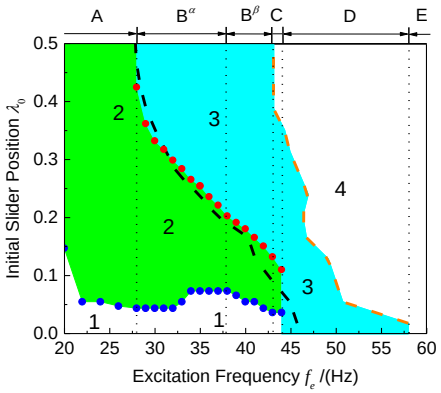

Fig.4 Critical initial positions of the slider without inclination: the blue and red dotted lines determine the boundaries of the region in which the slider is able to move toward centre (Region 2). The black and orange dashed lines are jump up (f_b) and jump down (f_f) frequencies when the slider is fixed in related positions.

5.2 Beam response and slider trajectory

Figs. 5(a) and 5(c) show the sider trajectories and beam responses at two typical frequencies (f_e=24 Hz and 27 Hz) in Sub-region A_1 (Region 1 below 28 Hz). The slider stays still at the initial positions near the clamping end of the beam (λ_0=0.074 for f_e=24 Hz and λ_0=0.037 for f_e=27 Hz). This is because the beam vibration amplitude and the curvature are not large enough to provide the slider adequate inertia force to overcome the static friction to move along the beam. The beam response is thus small. The same situations occur in Sub-regions B_1^{α}, B_1^{β} and C_1, which are shown in Figs. 6(a), 7(a) and 8(a), respectively. Note that the beam response increases while the slider does not move. This is attributed to the fact that it takes around 6 seconds for the shaker to reach the steady excitation level (10m s^{-2}). Hence, the increase of the beam response in these cases has nothing to do with the slider but just the increase of excitation in the startup stage. This exists in all the cases tested. In Sub-region A_2 (Region 2 below 28 Hz), the slider is able to move from side toward the centre, as shown in Figs. 5(b) and 5(d). Meanwhile, the beam vibration amplitude increases. In the final stable state, the slider stops

around the centre (λ=0.5). The beam response is amplified. This process is understandable by looking at the frequency responses in Fig. 3(a). Once the slider is initially placed at a position with sufficient vibration amplitude, the sufficient inertia force and thus F_T will drive the slider to move toward the centre, resulting the vibration amplitude increase and consequently the further increase in inertia force for the slider. If a disturbance is applied in the stable state, the beam-slider structure can recover its state quickly, because in Frequency Range A, only one energy orbit exists no matter where the slider is.

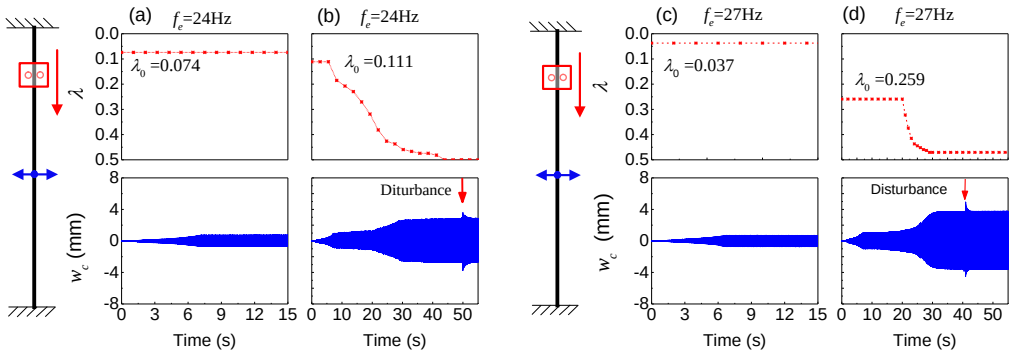

Fig.5 Time histories of slider trajectories (star-dashed line) and beam responses (blue solid line) under different excitation frequency f_e and slider initial position λ_0. (a), (c) two cases in Sub-region A_1; (b), (d) two cases in Sub-region A_2.

In Sub-region B_2^{α}, as shown in Fig. 6(b), the slider moves from the side toward the centre across the boundary (red dotted line in Fig. 4) and finally stop in Sub-region B_3^{α}. During this movement, beam vibration amplitude is amplified from 1 mm to 5.8 mm. This is because the slider initially starts from Region 2 can capture the high energy orbit when the slider is passing Region 3. However, the beam-slider structure might lose this high energy orbit easily once certain disturbance is applied, as shown in Fig. 6(b). Once it jumps to the low energy orbit, it cannot recover since the slider has already been in Region 3. This is similar to the situation that the beam-slider structure is excited from the static state in Sub-region B_3^{α}. In that case, the slider does not move and the system always stays at the low energy orbit, as shown in Fig. 6(c). In addition, by comparing the sliding trajectories in Figs. 5(b), 5(d) and 6(b), it is worth noting that the slider moves much quicker toward the centre when the beam response increases.

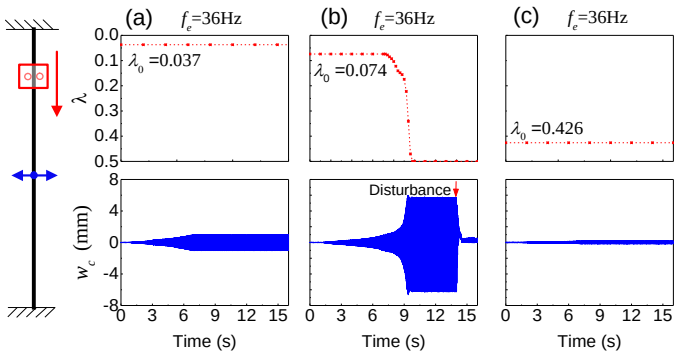

Fig.6 Time histories of slider trajectories (star-dashed line) and beam responses (blue solid line) under different excitation frequency f_e and slider initial position λ_0. (a) case in Sub-region B_1^{α}; (b) case in Sub-region B_2^{α}; (c) case in Sub-region B_3^{α}.

In Sub-region B_2^{β}, as shown in Fig. 7(b), the slider moves so quick to reach the centre (about 0.6 s) before the beam captures and sustains the high energy orbit. Consequently, distinguished from the case in Sub-region B_2^{α}, though the beam response increases dramatically during the brief time when the slider is moving, it cannot keep the large amplitude vibration after the slider stops around the centre and jumps to the low energy orbit. In Sub-region B_3^{β}, the slider cannot move and the beam vibrates in the low energy orbit, as shown in Fig. 7(c).

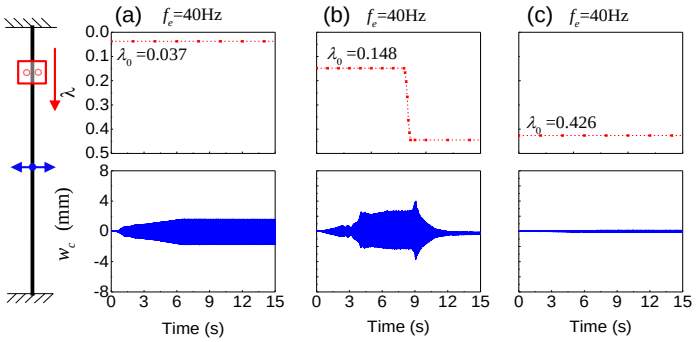

Fig.7 Time histories of slider trajectories (star-dashed line) and beam responses (blue solid line) under different excitation frequency f_e and slider initial position λ_0. (a) case in Sub-region B_1^{β}; (b) case in Sub-region B_2^{β}; (c) case in Sub-region B_3^{β}.

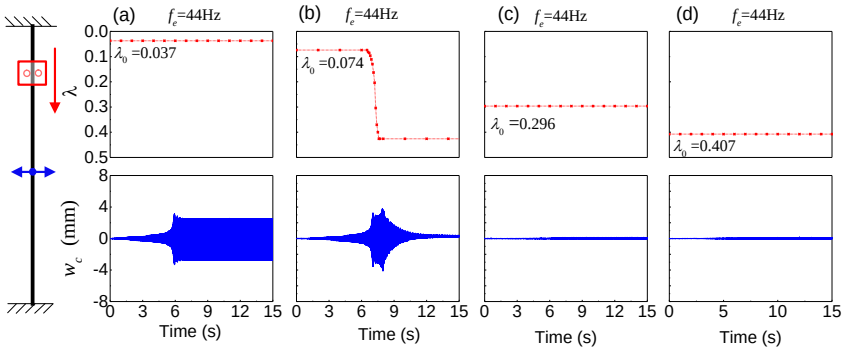

Fig.8 Time histories of slider trajectories (star-dashed line) and beam responses (blue solid line) under different excitation frequency f_e and slider initial position λ_0. (a) case in Sub-region C_1; (b) case in Sub-region C_2; (c) case in Sub-region C_3; (d) case in Sub-region C_4.

Frequency Range C is the most particular range as it spans all four regions, as shown in Fig. 4. The slider and beam behavior in Sub-region C_2 is similar to that in Sub-region B_2^{β}. However, except for the fast sliding speed, there is another reason for the small vibration in the final stage. When the slider reaches and stops in Sub-region C_4, there is only one energy orbit with small amplitude (this can be seen in Fig. 3(a)). As for Sub-regions C_3 and C_4, (Figs. 8(c) and 8(d)), the slider always stays still and the beam response is small. The difference between them can be observed by looking at the pink solid-dotted and dash-dotted lines in Fig. 3(b). The small amplitude for λ=0.296 is due to the system captures the low energy orbit initially, while for λ=0.407, the system has only one orbit with small amplitude. For λ=0.296 in Sub-region C_3, by some particular perturbation or forward sweep frequency, the system could catch the high energy orbit with large amplitude. While for λ=0.407 in Sub-region C_4, the beam small vibration amplitude has no chance to be enlarged. In the same way, these difference also exists between Sub-regions D_3 and D_4 even though the similar behavior is observed in Figs. 9(a) and 9(b).

In Sub-region E_4 (f_e>58 Hz), there is only one orbit no matter where the slider is located on the beam. As shown in Fig. 10, the slider cannot move and beam response is in small amplitude because the f_e is far beyond the natural frequency.

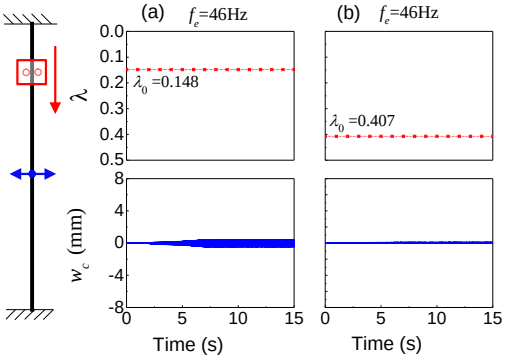

Fig.9 Time histories of slider trajectories (star-dashed line) and beam responses (blue solid line) under different excitation frequency f_e and slider initial position λ_0. (a) case in Sub-region D_3; (b) case in Sub-region D_4.

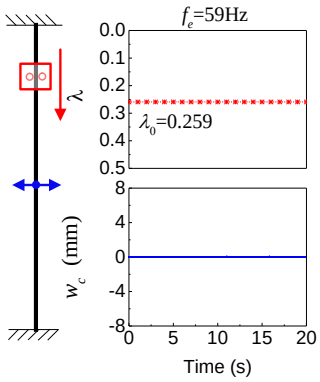

Fig.10 Time histories of slider trajectories (star-dashed line) and beam responses (blue solid line) under different excitation frequency f_e and slider initial position λ_0. Case in Sub-region E_4.

6. Improved Self-tuning with Inclination

As illustrated in previous sections, though the beam response increases significantly when the slider starts from Sub-region B_2^{α}, it is very sensitive to the disturbance. In the Sub-region B_2^{β}, the slider could move toward the centre but the beam eventually failed to maintain the high energy orbit. In addition, if the slider is initially placed in Sub-regions B_3^{α} and B_3^{β}, though high energy orbit does exist, it could not be captured when the beam is excited from the static status. In order to overcome this sensitivity to disturbance and best utilize the high energy orbit in Sub-regions B_3^{α} and B_3^{β}, the setup of the beam-slider structure is improved by introducing a small inclination of the clamped-clamped beam. The inclination is achieved by rotating the shaker by θ=3° and the excitation acceleration is still normal to the beam. This small inclination has negligible influence on the nonlinearity of the beam and the sweep FRFs if mass is fixed on the beam. However, the small gravitational component introduced will significantly affect the behavior of the slider and the beam responses. When the beam is in the static status or vibrating with a small amplitude, F_T could point to the clamped end of the beam in the most of the time during one vibration period and thus the slider moves toward the clamped end. Only when the inertial force of the slider is large enough (given large vibration amplitude) to overcome the static friction and the gravitational component along the beam, can the slider move from side toward the centre. In this way, for the multi-orbit regions, the small inclination could help the slider move back to the side once the beam jumps to low energy orbit due to certain disturbance and restart the self-tuning process. In other word, the system is anti-interference.

6.1 Critical positions for mass sliding on the beam

For the self-tuning capability, similar to the case without inclination, the whole region in

terms of the slider initial position (λ_0) and excitation frequency (f_e) can also be divided into 4 regions, as shown in Fig. 11. The blue dotted line is the boundary that determines whether the slider can move toward the lower end or the centre (λ=0.5) and the red dotted line is the critical position where the slider can reverse its moving direction when it slides toward the lower end. The jump up frequency f_b (black dashed line) and jump down frequency f_f (orange dashed line) are also shown in Fig. 11. Note that the lines of f_b and f_f are almost unchanged as compared to the case without inclination, which could be the proof that the small inclination has negligible influence on the nonlinearity of the beam. As compared to the case without inclination, Region 1 (below blue dotted line) becomes larger. This is because apart from the static friction, the slider has to overcome the extra small gravitational component along the beam to move toward the centre. The slider initially placed in this region will slide to the lower end rather than stay still at the initial position. Since the red dotted line is nearly the same as the case without inclination, Region 2 (between the blue and red dotted lines) becomes much smaller after the expansion of Region 1. There is only one orbit in this region. The slider starts from this region can move toward centre after overcoming the friction and small gravitational component. It is worth mentioning that, similar to the case without inclination, the red dotted line is almost the same as the line denoting f_b. In Region 3, between f_b and f_f, low energy and high energy orbits coexist. The difference in Region 3 for the cases without and with inclination (Figs. 4 and 11) lies in the behavior of the slider when the beam vibrates on the low energy orbit. For the case without inclination, the slider will stay still. While in the case with inclination, the slider will move toward the lower end due to gravity. Once the slider reaches the boundary between Region 2 and Region 3 (red dotted line in Fig. 11), the response on the unique orbit is relatively larger than that on the lower energy orbit in Region 3. As a result, the inertial force due to the relative large response can reverse direction of movement of the slider and drive it back to the centre. Since the slider is reversed from Region 2, it could capture the high energy orbit of Region 3. Since there is no Region 2 above 45 Hz, the slider can only move all the way to the lower end of the beam. In Region 4 (the right up side of the orange dashed line), only one energy orbit exists and the beam vibrates in a small amplitude. Because of the inclination, the slider initially placed in this region will move to the lower end of the beam as well.

Obviously, the performance of the beam-slider structure varies in different frequency ranges. Hence, these four regions are also further divided into various sub-regions. As compared to the case without inclination (Fig. 4), the boundary between Frequency Ranges b^{α} and b^{β} and the boundary between Frequency Ranges c and d in Fig. 11 shift to 39 Hz and 45Hz, respectively. Except for these changes, other Frequency ranges (a, d and e) keep the same as

those in the case without inclination (A, D and E). The most distinct difference in these sub-regions lies in that the slider can slide to the lower end by itself due to gravity when the beam amplitude is small. This characteristic improves the mutuality of the beam responses and the mass sliding trajectories. Therefore, all the sub-regions can be classified into four types by considering the performance of the entire beam-slider structure. For each type, the details about the slider movement and the beam response will be illustrated in the following section.

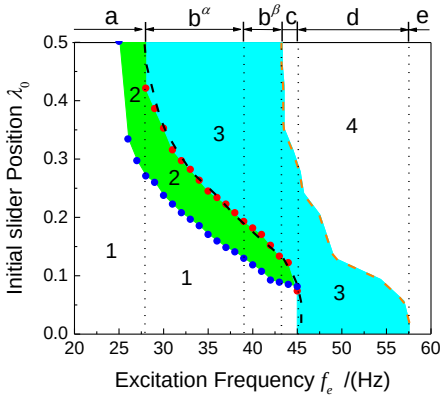

Fig.11 Critical initial positions of the slider with inclination: the blue and red dotted lines determine the boundaries of the region in which the slider is able to move toward the centre (Region 2). The black and orange dashed lines are jump up (f_b) and jump down (f_f) frequencies when the slider is fixed in related positions.

6.2 Beam response and slider trajectory

The first type of beam-slider behavior exists in Sub-regions a_1, b_1^{α}, b_1^{β}, c_1, d_3, d_4 and e, the slider moves toward the lower end of the beam due to the gravitational component until it is stopped by the clamp (λ=0.019). In Figs. 12(b), 13(a), 14(a) and 15(a), this type only occurs when the slider located near the lower end. But for Figs. 12(a), 16 and 17, the slider moves to the lower end of the beam no matter where the slider is initially placed. During this sliding movement, the beam response variation mainly depends on the excitation frequency. As shown previously, the lowest and highest natural frequencies of the beam are obtained when the slider located at the centre and the clamping end, respectively. If the excitation frequency is closer to the highest natural frequency, beam response will increase by the motion of slider, and vice versa. This is the reason why beam response in Figs. 12(a), 12(b), 14(a) and 15(a) decrease while beam responses in Figs. 16 and 17 increase. However, the response in the final state when the slider is blocked at the lower end, the final response is small.

The second type of beam-slider behavior exists only in Sub-region a_2, as shown in Fig. 12(c), the beam response is large enough to supply the inertial force for the slider moving toward the centre. As a result, the beam response is amplified gradually. In addition, since only one orbit

exists, given certain disturbance, this large response vibration state could recover quickly without the change of the slider position. The type of beam-slider structure behavior is quite similar to that in Sub-region A_2 in the case without inclination. Though the response is amplified, it is not large enough as compared to the response if the structure can capture the high energy orbit in Sub-region b_3^{α}.

The third type of beam-slider behavior exists in Sub-regions b_2^{α} and b_3^{α}, as shown in Figs. 13(b) and 13(c). The beam can keep its high energy orbit after the slider reaches the centre. If the beam is disturbed, the slider cannot hold its position and will slide toward the lower end. But, once the slider reaches the boundary of Region 2 and Region 3 (red dotted lined in Fig. 11), the beam can vibrate at a relatively large amplitude. As a result, the slider is driven toward the centre and the beam response is amplified again. In this way, the high energy orbit in Sub-region b_3^{α} can always be captured and is thus anti-interference.

The fourth type of beam-slider behavior exists in Sub-regions b_2^{β}, b_3^{β}, c_2, c_3 and c_4. As shown in Figs. 14(b), 14(c) and 15(b). The slider attempts to move toward the centre but cannot keep this tendency before the beam captures and holds the high energy orbit. Hence, the slider moves backward. Similar to the third type of beam-slider behavior, at the boundary of the Region 2 and Region 3 (red dotted line in Fig. 11), the beam jumps up to obtain a relatively large vibration amplitude and makes the slider move toward the centre again. Therefore, the slider keeps moving back and forth along the beam and the amplitude of beam response rises and drops periodically.

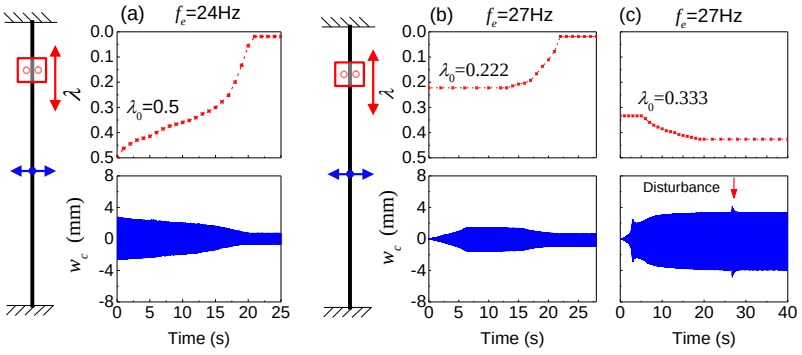

Fig.12 Time histories of slider trajectories (star-dashed line) and beam responses (blue solid line) under different excitation frequency f_e and slider initial position λ_0. (a), (b) two cases in Sub-region a_1; (c) case in Sub-region a_2.

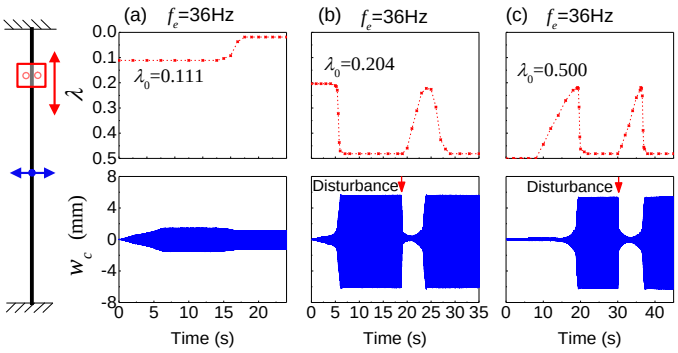

Fig.13 Time histories of slider trajectories (star-dashed line) and beam responses (blue solid line) under different excitation frequency f_e and slider initial position λ_0. (a) case in Sub-region b_1^{α}; (b) case in Sub-region b_2^{α}; (c) case in Sub-region b_3^{α}.

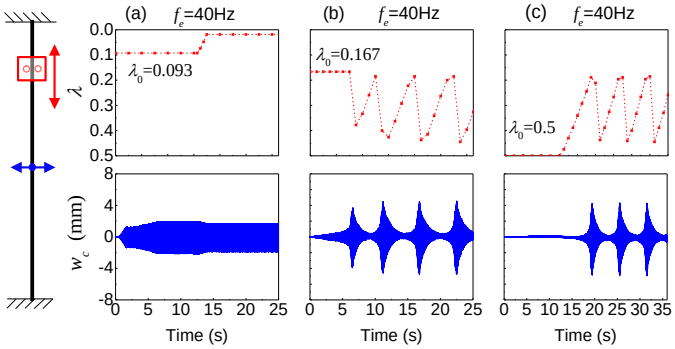

Fig.14 Time histories of slider trajectories (star-dashed line) and beam responses (blue solid line) under different excitation frequency f_e and slider initial position λ_0. (a) case in Sub-region b_1^{β}; (b) case in Sub-region b_2^{β}; (c) case in Sub-region b_3^{β}.

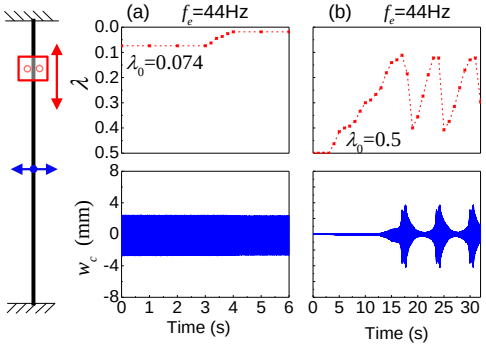

Fig.15 Time histories of slider trajectories (star-dashed line) and beam responses (blue solid line) under different excitation frequency f_e and slider initial position λ_0. (a) case in Sub-region c_1; (b) case in Sub-region c_2, c_3 and c_4.

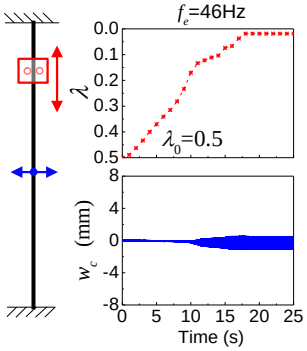

Fig.16 Time histories of slider trajectories (star-dashed line) and beam responses (blue solid line) under different excitation frequency f_e and slider initial position λ_0. Case in Sub-region d_3 and d_4.

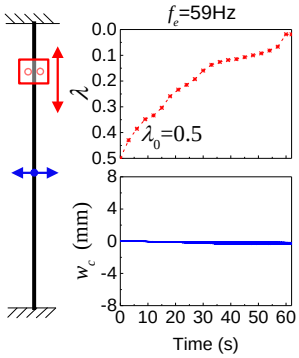

Fig.17 Time histories of slider trajectories (star-dashed line) and beam responses (blue solid line) under different excitation frequency f_e and slider initial position λ_0. Case in Sub-region e.

In summary, the first type of beam-slider behavior fails to achieve self-tuning for large response. For the second type of beam-slider behavior, it is nearly the same as that in Sub-region A2 in the case without inclination. However, though, the beam response is magnified as the slider reaches the centre, it is still limited. For the third type of beam-slider behavior, the beam can capture and maintain the high energy orbit to achieve self-tuning and anti-inference could be guaranteed. In addition, the slider initial position region for successful tuning embraces Sub-region b_3^{α}. For the fourth type of beam-slider behavior, the slider always moves back and forth along the beam and beam response rises and drops periodically. This particular type is not as useful as the third type. But the response of beam is better than that in Sub-region B_2^{β} in the case without inclination.

6.3 Discussion

Given that the clamped-clamped beam in the case without inclination is symmetric, the tunable regions are symmetric about λ_0=0.5. Hence, only half of the successful tuning regions are shown in Fig. 18(a). While in the case with inclination, no matter what the status of the beam is, the slider that starts from the higher half side of the beam is able to move toward the centre of the beam. After the slider reaches the centre of the beam, the behavior of the beam-slider structure is the same as the behavior when the slider starts from the lower half side of the beam. Hence, only the lower half side of the tunable regions for the case with inclination are shown in Fig. 18(b). Fig. 18(a) shows that only when the slider starts from the green region (including the shadow green region), can the final response of beam be amplified. Since the slider starting from B_2^{α} (shadow green region) will eventually stay in the multi-orbit region B_3^{α}, the amplified beam response benefiting from the high energy orbit is quite sensitive to the disturbance. As for the other regions, the final steady state response of the

beam could not be amplified.

In the case with inclination (Fig. 18(b)), the slider in the green region can slide toward the centre of the beam and keep the beam vibrating in large amplitude. Even though the system is disturbed, it can recover and restart the self-tuning. This property makes the final amplified beam response anti-interference. Additionally, the slider that starts from the grey region can always move back and forth between the centre and the lower end. This motion also makes the beam vibration amplitude rises up and drops periodically.

Comparing the regions in Figs. 18(a) and 18(b), the inclination changes the tunable regions in four aspects. First, the tunable Sub-region A_2 where only one energy orbit exists is significantly shrunk to Sub-region a_2. However, as demonstrated in section 6.2, the magnification of beam response after self-tuning in this lost region is very limited.

Second, the region for capturing the high energy orbit extends to the multi-orbit region b_3^{α}. It should be mentioned that this region becomes continuous, which makes it more feasible for setting slider's initial position. Furthermore, the final significantly amplified beam response benefiting from the high energy orbit in Sub-regions b_2^{α} and b_3^{α} are anti-inference, which is much more advantageous over the Sub-region B_2^{α} in the case without inclination.

Third, due to the inclination that can reduce the speed of the slider due to the small gravitational component when it moves toward the centre, the higher boundary of green self-tuning region shifts from 37 Hz to 39 Hz. This also confirms the reason why the beam cannot keep vibrating on the high energy orbit when the slider moves to the centre in Sub-region B_2^{β}: the slider moves so fast that the beam has not sufficient time to sustain the high energy orbit.

Finally, even though the beam in the grey region cannot keep vibrating on the high energy orbit, the slider always moves back and forth along the beam and the beam response swaps between large amplitude and low amplitude periodically. This additional region is not as useful as the green self-tuning region but is better than the case without inclination.

The inclination that introduces the gravitational component to the structure helps enable the slider to move back to the side when the beam amplitude decrease and reset the slider to the successful self-tuning region. Though part of the less efficient sub-region was sacrificed (A2 shrunk to a2), the gained broader region of self-tuning and maintaining high energy orbit response with anti-interference property makes the proposed resonator structure very attractive for the potential design of broadband energy harvesting systems. In addition, Regions b_2^{α} and b_3^{α} are the regions where the slider can enable the beam to catch the high

energy orbit. The possible way to further extend this region is as follow: Make the beam and the slider smoother to reduce friction between them. In this way, the inclination could be smaller for the slider to overcome the friction and thus less region a_2 and region b_2^{α} will be sacrificed.

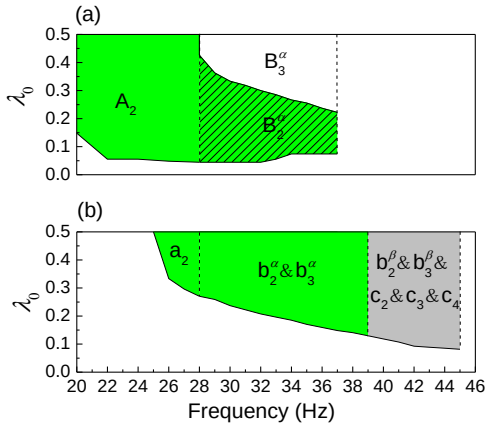

Fig.18 Comparison of self-tuning regions (a) without and (b) with inclination.

7. Conclusions

This work experimentally investigated the passive self-tuning process of the beam-slider structure without and with a small inclination. The clamped-clamped beam has hardening nonlinearity. It is revealed that the slider could help acquire the high energy orbit in the beam nonlinear response when it is initially placed in the certain region.

In the case without inclination, though the beam can capture the high energy orbit initially from Sub-region B_2^{α} and vibrate in significantly amplified amplitude when it finally settles in Sub-region B_3^{α}, the desired status can be lost easily given certain disturbance. To overcome this drawback, an improved design with a small inclination in installation is proposed. This inclination is so small that it does not prevent the slider moving toward the centre given sufficient vibration amplitude of the beam, and it does not affect the frequency response when the slider stops, either. In addition, when the vibration amplitude decreases, the slider could move back toward the side due to the gravity and restart the self-tuning process from the successful tuning region. This ensures the nonlinear beam to capture the high energy orbit passively even though the beam-slider structure is excited from low energy orbit. In this way, the significantly amplified vibration response is anti-interference in Sub-region b_3^{α}. What is more, the phenomenon that the slider moves back and forth along the beam and beam vibration response swaps between large amplitude and low amplitude periodically is observed in 39 Hz-45 Hz.

In summary, the improved beam-slider resonator structure with inclination can promote the beam response by capturing and maintaining the high energy orbit with anti-interference capability. The proposed proof-of-concept beam-slider resonator with inclination can achieve truly passive self-tuning and provide large response vibrations between 25 Hz-39 Hz.

Acknowledgements

The authors gratefully acknowledge the supports from the National Natural Science Foundation of China (No. 51375103) and China Scholarship Council (No. 201706680013).

References

[1] Tang L, Yang Y, Soh CK. Broadband vibration energy harvesting techniques. Advances in energy harvesting methods: Springer; 2013. p. 17-61.

[2] Daqaq MF, Masana R, Erturk A, Quinn DD. On the role of nonlinearities in vibratory energy harvesting: a critical review and discussion. Applied Mechanics Reviews 2014;66:040801.

[3] Erturk A, Inman DJ. Broadband piezoelectric power generation on high-energy orbits of the bistable Duffing oscillator with electromechanical coupling. Journal of Sound and Vibration 2011;330:2339-53.

[4] Harne RL, Wang KW. A review of the recent research on vibration energy harvesting via bistable systems. Smart Materials and Structures 2013;22.

[5] Lan CB, Tang LH, Qin WY. Obtaining high-energy responses of nonlinear piezoelectric energy harvester by voltage impulse perturbations. European Physical Journal-Applied Physics. 2017;79.

[6] Ramlan R, Brennan MJ, Mace BR, Kovacic I. Potential benefits of a non-linear stiffness in an energy harvesting device. Nonlinear Dynamics 2009;59:545-58.

[7] Zhou SX, Cao JY, Inman DJ, Liu SS, Wang W, Lin J. Impact-induced high-energy orbits of nonlinear energy harvesters. Applied Physics Letters 2015;106.

[8] Wang GQ, Liao WH. A bistable piezoelectric oscillator with an elastic magnifier for energy harvesting enhancement. Journal of Intelligent Material Systems and Structures 2017;28:392-407.

[9] Mallick D, Amann A, Roy S. Surfing the High Energy Output Branch of Nonlinear Energy Harvesters. Phys Rev Lett. 2016;117:197701.

[10] Masuda A, Senda A, Sanada T, Sone A. Global stabilization of high-energy response for a Duffing-type wideband nonlinear energy harvester via self-excitation and entrainment. Journal of Intelligent Material Systems and Structures 2013;24:1598-612.

[11] Sebald G, Kuwano H, Guyomar D, Ducharne B. Experimental Duffing oscillator for broadband piezoelectric energy harvesting. Smart Materials and Structures 2011;20:102001.

[12] Sebald G, Kuwano H, Guyomar D, Ducharne B. Simulation of a Duffing oscillator for broadband piezoelectric energy harvesting. Smart Materials and Structures 2011;20:075022.

[13] Gu L, Livermore C. Passive self-tuning energy harvester for extracting energy from rotational motion. Applied Physics Letters 2010;97:081904.

[14] Jo S-E, Kim M-S, Kim Y-J. A resonant frequency switching scheme of a cantilever based on polyvinylidene fluoride for vibration energy harvesting. Smart Materials and Structures 2012;21:015007.

[15] Miller LM. Micro-scale piezoelectric vibration energy harvesting: From fixed-frequency to adaptable-frequency devices: University of California, Berkeley; 2012.

[16] Miller LM, Pillatsch P, Halvorsen E, Wright PK, Yeatman EM, Holmes AS. Experimental passive self-tuning behavior of a beam resonator with sliding proof mass. Journal of Sound and Vibration 2013;332:7142-52.

[17] Pillatsch P, Miller LM, Halvorsen E, Wright PK, Yeatman EM, Holmes AS. Self-tuning behavior of a clamped-clamped beam with sliding proof mass for broadband energy harvesting. Journal of Physics: Conference Series 2013;476:012068.

[18] Gregg CG, Pillatsch P, Wright PK. Passively Self-Tuning Piezoelectric Energy Harvesting System. Journal of Physics: Conference Series 2014;557:012123.

[19] Staaf LGH, Smith AD, Köhler E, Lundgren P, Folkow PD, Enoksson P. Achieving increased bandwidth for 4 degree of freedom self-tuning energy harvester. Journal of Sound and Vibration 2018;420:165-73.

[20] Staaf LGH, Smith AD, Lundgren P, Folkow PD, Enoksson P. Effective piezoelectric energy harvesting with bandwidth enhancement by assymetry augmented self-tuning of conjoined cantilevers. International Journal of Mechanical Sciences 2019;150:1-11.

[21] Krack M, Aboulfotoh N, Twiefel J, Wallaschek J, Bergman LA, Vakakis AF. Toward understanding the self-adaptive dynamics of a harmonically forced beam with a sliding mass. Archive of Applied Mechanics. 2016;87:699-720.

[22] Wagg D, Neild S. Nonlinear vibration with control: Springer; 2009.